Stem Cell Reports
Article

ISSCR

OPEN ACCESS

The histone H3.3 chaperone HIRA restrains erythroid-biased differentiation of adult hematopoietic stem cells

Rebecca L. Murdaugh,[1] Kevin A. Hoegenauer,[2] Ayumi Kitano,[2] Matthew V. Holt,[3,4] Matthew C. Hill,[1] Xiangguo Shi,[2] Jonathan F. Tiessen,[1] Richard Chapple,[2] Tianyuan Hu,[2] Yu-Jung Tseng,[5] Angelique Lin,[2] James F. Martin,[1,6,7] Nicolas L. Young,[3,4,8] and Daisuke Nakada[1,2,5,*]

[1]Graduate Program in Developmental Biology, Baylor College of Medicine, Houston, TX 77030, USA
[2]Department of Molecular and Human Genetics, Baylor College of Medicine, Houston, TX 77030, USA
[3]Graduate Program in Biochemistry and Molecular Biology, Baylor College of Medicine, Houston, TX 77030, USA
[4]Verna & Marrs McLean Department of Biochemistry & Molecular Biology, Baylor College of Medicine, Houston, TX 77030, USA
[5]Graduate Program in Translational Biology and Molecular Medicine, Baylor College of Medicine, Houston, TX 77030, USA
[6]Department of Molecular Physiology and Biophysics, Baylor College of Medicine, Houston, TX 77030, USA
[7]Texas Heart Institute, Houston, TX 77030, USA
[8]Department of Molecular and Cellular Biology, Baylor College of Medicine, Houston, TX 77030, USA
*Correspondence: nakada@bcm.edu
https://doi.org/10.1016/j.stemcr.2021.06.009

SUMMARY

Histone variants contribute to the complexity of the chromatin landscape and play an integral role in defining DNA domains and regulating gene expression. The histone H3 variant H3.3 is incorporated into genic elements independent of DNA replication by its chaperone HIRA. Here we demonstrate that *Hira* is required for the self-renewal of adult hematopoietic stem cells (HSCs) and to restrain erythroid differentiation. Deletion of *Hira* led to rapid depletion of HSCs while differentiated hematopoietic cells remained largely unaffected. Depletion of HSCs after *Hira* deletion was accompanied by increased expression of bivalent and erythroid genes, which was exacerbated upon cell division and paralleled increased erythroid differentiation. Assessing H3.3 occupancy identified a subset of polycomb-repressed chromatin in HSCs that depends on HIRA to maintain the inaccessible, H3.3-occupied state for gene repression. HIRA-dependent H3.3 incorporation thus defines distinct repressive chromatin that represses erythroid differentiation of HSCs.

INTRODUCTION

The adult hematopoietic system is sustained by the self-renewal and differentiation of a small pool of hematopoietic stem cells (HSCs) that are essential to regenerate the hematopoietic system upon transplantation or after injury (Laurenti and Gottgens, 2018; Pietras, 2017). A number of epigenetic regulators that modify DNA or histones have been shown to be essential for HSC fate decision, such as DNMT3A, polycomb group proteins BMI1 and EZH2, or histone acetyltransferases EP300 and CBP (Challen et al., 2011; Lessard and Sauvageau, 2003; Mochizuki-Kashio et al., 2011; Park et al., 2003; Rebel et al., 2002; Sandberg et al., 2005; Xie et al., 2014). In addition to these epigenetic modifications exerted upon DNA or histones, variant forms of histones provide another layer of epigenetic information to control gene expression and cell fate (Hake and Allis, 2006; Henikoff and Smith, 2015; Lara-Astiaso et al., 2014; Martire and Banaszynski, 2020). However, the role of histone variant incorporation as an epigenetic mechanism regulating HSC fate determination remains largely unexplored.

The three main variants of histone H3 in mammalian cells—H3.1, H3.2, and H3.3—each have distinct enrichment patterns established by corresponding histone chaperones (Burgess and Zhang, 2013; Maze et al., 2014). Histones H3.1 and H3.2 are synthesized and deposited into chromatin during S phase (termed replication-dependent incorporation). In contrast, histone H3.3 is expressed and incorporated into chromatin throughout the cell cycle (termed replication-independent incorporation). Differential deposition occurs despite the fact that H3.3 differs from H3.1 and H3.2 by only four or five amino acids and depends on chaperones specific to either H3.1/H3.2 or H3.3. The distinct mechanisms by which replication-dependent and -independent histone H3 variants are incorporated into chromatin suggest that quiescent adult HSCs and actively dividing precursor cells may differentially depend on histone variant chaperones.

The incorporation of DNA replication-dependent H3.1 and H3.2 is governed by the CAF1 complex, while deposition of replication-independent H3.3 is mediated by either the HIRA or the DAXX/ATRX complex (Burgess and Zhang, 2013; Goldberg et al., 2010). Incorporation of H3.3 by HIRA occurs at the promoters, enhancers, and gene bodies of actively expressed genes as well as at bivalent promoters, CTCF binding sites, and retroviral elements (Elsasser et al., 2015; Goldberg et al., 2010; Ray-Gallet et al., 2011). Conversely, DAXX/ATRX mainly mediates incorporation of H3.3 into telomeres and pericentromeric DNA. The

presence of H3.3 at bivalent promoters is of particular interest in the context of stem cell biology as a possible mechanism regulating differentiation potential of stem cells and occurs through recruitment of PRC2 by HIRA (Banaszynski et al., 2013). Regulation of H3.3 by the HIRA complex may therefore be an important epigenetic mechanism underlying HSC potential.

In this study, we demonstrate that HIRA is essential for HSC self-renewal. Deletion of *Hira* from the hematopoietic system revealed that, while *Hira* is dispensable for fetal liver HSCs, it is essential for adult HSC maintenance. Upon loss of *Hira*, adult HSCs become rapidly depleted and exhibit erythroid-biased differentiation. Genome-wide histone H3.3 profiling also demonstrated that H3.3 occupancy defines bivalent promoters and a subset of polycomb-repressed chromatin that becomes derepressed upon *Hira* deletion. Transcriptomic changes associated with HSC division show that erythroid-differentiation genes become derepressed after division in the absence of HIRA. Together, our data establish a previously unappreciated role for *Hira* in safeguarding HSC self-renewal by preventing precocious erythroid differentiation.

RESULTS

Hira is essential for adult but not fetal HSC maintenance

To study the role of histone H3.3 regulation in hematopoietic stem and progenitor cells (HSPCs), we first examined the levels of the histone H3 variants (H3.1, H3.2, and H3.3). We performed high-performance liquid chromatography (HPLC) analyses with whole bone marrow (WBM) cells and lineage$^-$c-kit$^+$ (LK) cells sorted from adult mice (Figures 1A and S1A). In WBM cells, H3.2 was the predominant H3 variant, constituting ~55% of total H3, followed by H3.3 (~35%) and H3.1 (~10%), while H3.3 was the predominant H3 variant in HSPCs (~60%). Although the LK population includes not only primitive HSPCs but also lineage-restricted precursor cells, these results suggest that histone H3.3 and its chaperones may have important functions in undifferentiated hematopoietic cells.

We then focused on the histone H3.3 chaperone HIRA and assessed the relative expression of *Hira* and the two genes encoding histone H3.3, *H3f3a* and *H3f3b*, in fetal liver and adult bone marrow by quantitative PCR (Figures S1B and S1C). Consistent with our HPLC data, bone marrow HSPCs showed a trend toward increased expression of *H3f3b* compared with WBM cells. We also observed higher levels of *Hira* expression in adult and fetal HSPCs compared with the bulk of hematopoietic cells, but the expression of *Hira*, *H3f3a*, or *H3f3b* was not different between fetal and adult HSCs (Figure S1D).

We then generated *Vav1-iCre; Hira$^{fl/fl}$* mice to delete *Hira* during early hematopoietic development (Georgiades et al., 2002) (Figures 1B and S1D). Loss of HIRA protein in hematopoietic cells after *Hira* deletion with *Vav1-iCre* was confirmed by immunoblotting (Figures 1C, S1E, and S1F). The number of hematopoietic cells in the E14.5–16.5 fetal liver, livers of newborn pups (P0), and bone marrow of 1–2 week old neonates was not affected by deleting *Hira* (Figure 1D). However, the bone marrow cellularity of *Vav1-iCre; Hira$^{fl/fl}$* mice began to show significant reduction compared with that of control *Hira$^{fl/fl}$* mice at 3–4 weeks of age, which was exaggerated with age in mice 6 months or older (Figure 1D). The cellularity of the spleens was also reduced in adult mice (Figure 1D). The frequency of Ter119$^+$ erythroid cells was increased in both the bone marrow and the spleens of *Vav1-iCre; Hira$^{fl/fl}$* mice, and the total numbers of bone marrow Ter119$^+$ erythroid cells, Mac-1/Gr-1$^+$ myeloid cells, B220$^+$ B cells, and CD3$^+$ T cells were all reduced with age as *Vav1-iCre; Hira$^{fl/fl}$* mice exhibited reduced bone marrow cellularity (Figures 1E and S1G). In contrast, the spleens of *Vav1-iCre; Hira$^{fl/fl}$* mice showed increased myeloid and erythroid cell numbers as they aged, despite reduced spleen cellularity (Figures 1E and S1G). *Vav1-iCre; Hira$^{fl/fl}$* mice showed reduced viability at ~6 months of age, exhibiting early-onset leukopenia and late-onset thrombocytopenia (Figures 1F and 1G). Thus, *Hira* is essential for adult hematopoiesis but largely dispensable for fetal liver hematopoiesis.

To further explore the role of *Hira* in hematopoiesis, we analyzed the most primitive compartments within the lineage$^-$c-kit$^+$Sca-1$^+$ (LSK) population, namely CD150$^+$CD48$^-$ LSK HSCs and CD150$^-$CD48$^-$ LSK multipotent progenitors (MPPs) (Kiel et al., 2005; Oguro et al., 2013) of *Vav1-iCre; Hira$^{fl/fl}$* mice. Consistent with our finding that *Hira* is dispensable for maintaining fetal liver cellularity, *Hira* deletion did not change the frequencies or cell numbers of HSCs, MPPs, or LSK cells in the fetal liver (Figures 1H, S1H, and S1I). However, within 1–2 weeks of birth, HSCs, MPPs, and LSK cells in *Vav1-iCre; Hira$^{fl/fl}$* mice became severely depleted, preceding the depletion of hematopoietic cells in the bone marrow and in the spleen. In contrast, the numbers of lineage-restricted progenitors, such as common lymphoid progenitors, common myeloid progenitors, and granulocyte-macrophage progenitors, did not become reduced until 1–4 months of age in *Vav1-iCre; Hira$^{fl/fl}$* mice (Figures S1K–S1M). Interestingly, although the total numbers of megakaryocyte-erythroid progenitors (MEPs) were similar to controls, their frequency was increased, suggesting that the megakaryocytic-erythroid lineage is less affected by *Hira* deletion than the lymphoid and granulocytic-monocytic lineages (Figures 1I and S1M). These results establish that *Hira* is essential to maintain adult HSCs, but fetal liver HSCs can persist through embryonic development independent of *Hira*.

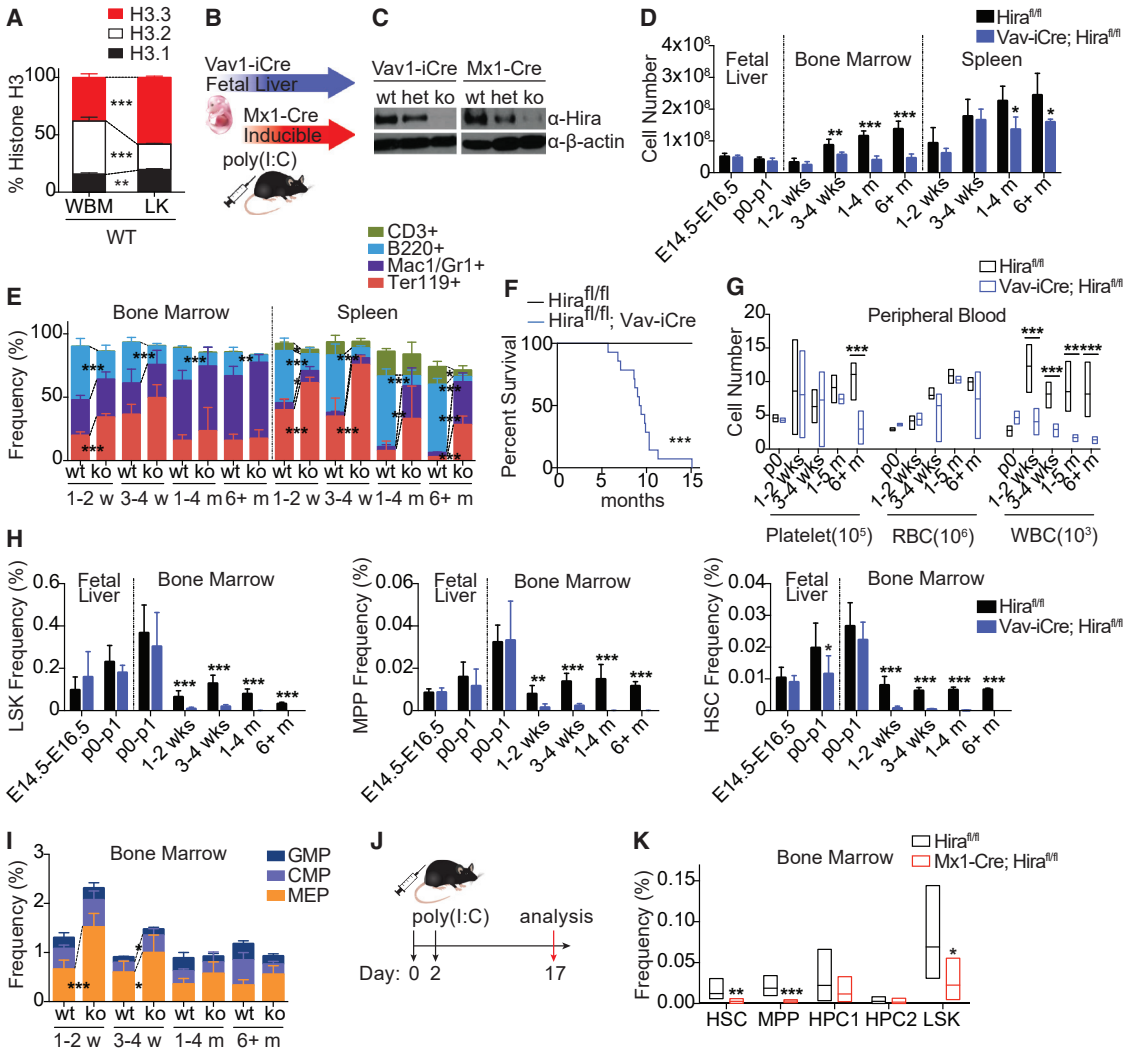

Figure 1. *Hira* is essential for adult but not fetal HSC maintenance

(A) Quantification of the three major histone H3 variants in WBM or LK cells from wild-type (WT) mice as assessed by HPLC (n = 3 mice).

(B) A diagram showing two mouse models of *Hira* conditional knockout in the hematopoietic system with *Vav1-iCre* and *Mx1-Cre*.

(C) Immunoblotting assay shows that *Hira* deletion reduced HIRA protein levels in the bone marrow (BM) cells after deleting *Hira*.

(D) Cellularity of fetal liver, BM, and spleen from *Vav1-iCre; Hira*$^{fl/fl}$ and *Hira*$^{fl/fl}$ mice at different developmental time points (n = 3–8 mice).

(E) Frequency of CD3$^+$ T cells, B220$^+$ B cells, Mac1$^+$Gr-1$^+$ myeloid cells, and Ter119$^+$ erythroid cells in *Vav1-iCre; Hira*$^{fl/fl}$ and *Hira*$^{fl/fl}$ mice in the BM and spleen at the indicated ages (n = 4–7 mice).

(F) Survival curve for *Vav1-iCre; Hira*$^{fl/fl}$ and *Hira*$^{fl/fl}$ mice (n = 14).

(G) Complete blood count of peripheral blood in *Vav1-iCre; Hira*$^{fl/fl}$ and *Hira*$^{fl/fl}$ mice at the indicated ages (RBC, red blood cell; WBC, white blood cell) (n = 3–7 mice).

(H) The total numbers of LSKs, MPPs, and HSCs in the liver or BM of *Vav1-iCre; Hira*$^{fl/fl}$ and *Hira*$^{fl/fl}$ mice at the indicated ages (n = 3–8 mice).

(I) Frequency of MEPs, common myeloid progenitors (CMP), and granulocyte-macrophage progenitors (GMP) in the BM of *Vav1-iCre; Hira*$^{fl/fl}$ and *Hira*$^{fl/fl}$ mice at different developmental time points (n = 4–7 mice).

(J) Diagram of the poly(I:C) treatment schedule. We treated mice with two doses of poly(I:C) and analyzed the mice 17 days after the first injection.

(K) Frequency of HSC, MPP, HPC1, HPC2, and LSK cells in *Mx1-Cre; Hira*$^{fl/fl}$ and *Hira*$^{fl/fl}$ mice 17 days after treatment with poly(I:C) (n = 6–9 mice).

All data represent the mean ± standard deviation; *p < 0.05, **p < 0.01, and ***p < 0.001 by Student's t test, except for the comparison of the survival curves, in which the significance was accessed by a log-rank test.

See also Figure S1.

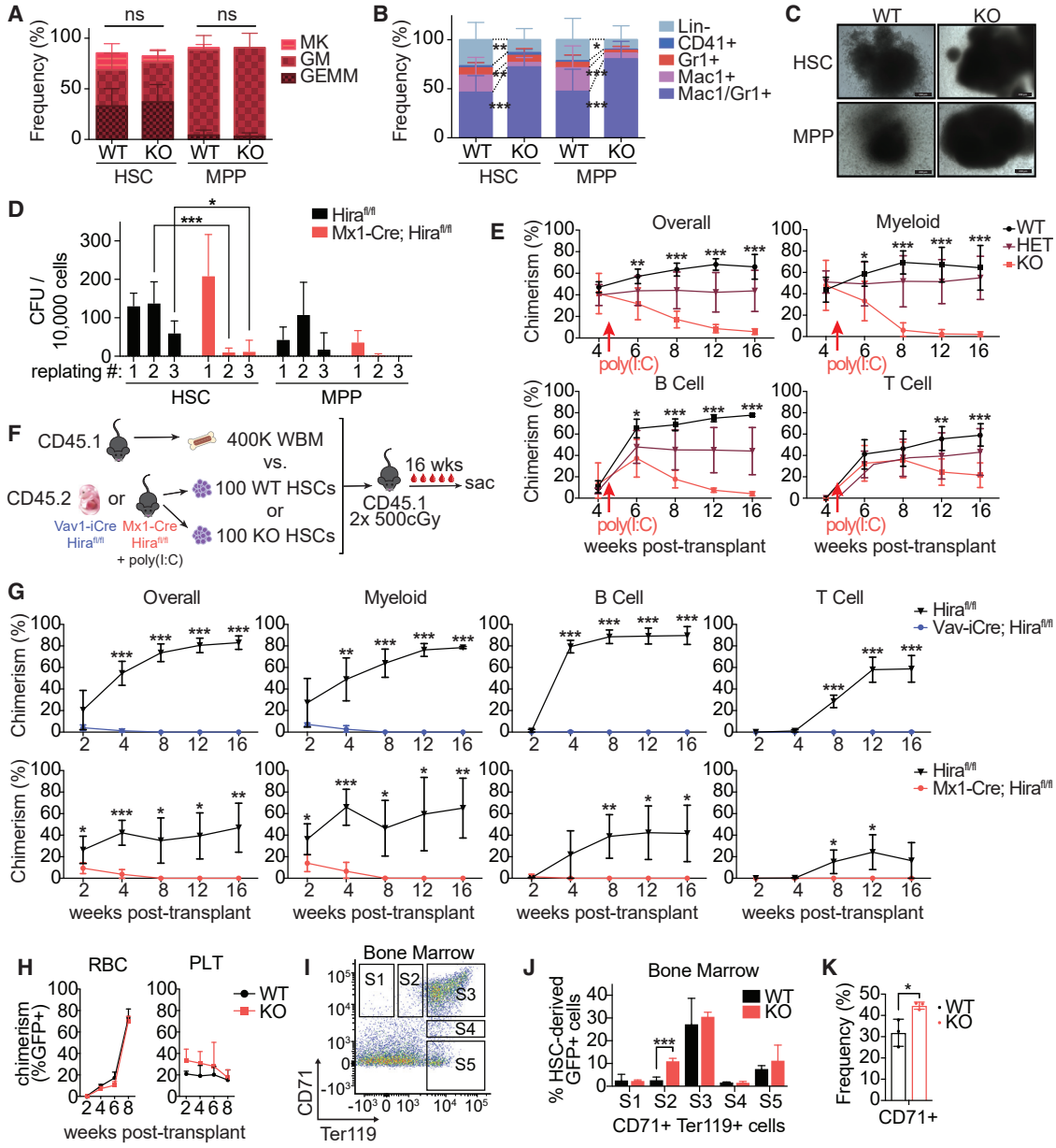

Figure 2. HIRA prevents precocious differentiation of HSCs

(A) Colony-forming assays with singly sorted HSCs/MPPs from either *Hira*$^{fl/fl}$ (WT) or *Mx1-Cre; Hira*$^{fl/fl}$ (KO) mice and scored for colonies containing granulocytes, erythrocytes, monocytes, and megakaryocytes (GEMM), granulocytes and monocytes (GM), or only megakaryocytes (MK) (n = 6–13 mice).

(B) Frequencies of cells with the indicated marker expression within colonies from (A).

(C) Representative images of colonies formed by HSCs or MPPs from WT and KO mice.

(D) Number of secondary colonies produced from HSCs and MPPs in three serial replatings of 10,000 cells (n = 3 mice).

(E) Adult WBM competitive transplant assays with 10^6 untreated *Hira*$^{fl/fl}$ (WT), *Mx1-Cre; Hira*$^{+/fl}$ (HET), or *Mx1-Cre; Hira*$^{fl/fl}$ (KO, all CD45.2$^+$) donor BM cells competing against 5 × 10^5 CD45.1$^+$ BM cells in CD45.1 recipient mice (n = 5 mice). Recipient mice were treated with seven injections of poly(I:C) 4 weeks after transplant (red arrow). Frequencies of CD45.2$^+$ WBCs in the peripheral blood tracked over 4 months post-transplantation are shown with statistical significance assessed between WT and KO.

(F) Diagram showing the experimental strategy used for the fetal liver (FL) and adult HSC competitive transplants in (G).

(G) Donor-derived chimerism of CD45.2$^+$ WBCs (overall) and myeloid, B, and T cells in the peripheral blood tracked over 4 months post-transplantation for FL and adult HSC competitive transplants from (F) (n = 5 mice).

(legend continued on next page)

The rapid depletion of adult HSCs in *Vav1-iCre; Hira*$^{fl/fl}$ mice within 1–2 weeks of birth prompted us to then test how adult HSCs respond to acute deletion of *Hira*. To this end, we generated *Mx1-Cre; Hira*$^{fl/fl}$ mice and conditionally deleted *Hira* by administering two doses of polyinosinic:-polycytidylic acid (poly(I:C)) to 6–8 week old mice and analyzed the mice 15 days after the last injection (Figures 1B, 1C, and 1J). HSCs and MPPs were severely depleted shortly after an acute deletion of *Hira* (Figure 1K). HPC1 (LSKCD150^{-}CD48^{+}) but not HPC2 (LSKCD150^{+}CD48^{+}) also showed a trend toward reduced frequency in the bone marrow, contributing to the reduced overall frequency of the LSK population (Figure 1K). These results reveal a critical role for *Hira* in the maintenance of adult HSCs.

Hira is essential for HSC self-renewal

We next assessed whether depletion of *Hira*-deficient HSCs was due to increased cell death or differentiation. Annexin-V staining or bromodeoxyuridine incorporation assays did not reveal any changes in apoptosis or cell division, respectively, in HSCs or MPPs after *Hira* deletion (Figures S2A and S2B). Sorting single HSCs or MPPs into semisolid medium showed that *Hira*-deficient HSCs and MPPs formed larger colonies with more cells that expressed granulocytic-monocytic lineage markers and fewer lineage^{-} cells with clonogenicity similar to that of wild-type HSCs (Figures 2A–2D, S2C, and S2D). Serial replating of these colonies showed that *Hira*-deficient primary colonies produced fewer colonies than wild type, despite having produced more cells initially (Figures 2D and S2E). These results suggest that loss of *Hira* increases the propensity of HSCs to differentiate at the cost of self-renewal.

We next performed competitive transplantation assays to determine the reconstitution potential of HSCs (Figures S2F and S2G). We first transplanted E16.5 whole fetal liver cells from *Vav1-Cre; Hira*$^{fl/fl}$ and control *Hira*$^{fl/fl}$ embryos along with competitor adult bone marrow cells into lethally irradiated recipient mice (Figure S2F). *Vav1-Cre; Hira*$^{fl/fl}$ fetal liver cells were severely compromised in their ability to reconstitute the hematopoietic system upon transplantation, exhibiting negligible reconstitution in recipient mice (Figure S2H). We then treated *Mx1-Cre; Hira*$^{fl/fl}$, *Mx1-Cre; Hira*$^{+/fl}$, and control *Hira*$^{fl/fl}$ mice with poly(I:C) 1 week prior to performing a WBM competitive transplantation. Consistent with the severe HSC depletion observed shortly after deleting *Hira*, we observed negligible levels of reconstitution from the *Hira*-deficient bone marrow cells, and none of the recipient mice showed long-term multilineage reconstitution (Figure S2I). *Mx1-Cre* is activated in bone marrow stromal cells by poly(I:C) (Park et al., 2012), raising the possibility that *Hira* deletion negatively affected HSCs in an HSC-extrinsic manner. To assess this possibility, we transplanted bone marrow cells from untreated *Mx1-Cre; Hira*$^{fl/fl}$, *Mx1-Cre; Hira*$^{+/fl}$, and control *Hira*$^{fl/fl}$ mice and then treated the recipient mice with poly(I:C) 1 month after transplantation. Although the initial engraftment was similar between the three groups, poly(I:C) administration reduced reconstitution by *Mx1-Cre; Hira*$^{fl/fl}$ cells in all lineages, leaving none of the recipient mice with multilineage reconstitution (Figure 2E). Thus, *Hira* is required within HSCs to support multilineage reconstitution potential.

Finally, we performed competitive HSC transplantation assays to directly assess the reconstitution potential of *Hira*-deficient HSCs. We sorted 100 HSCs from the fetal liver of E16.5 *Vav1-iCre; Hira*$^{fl/fl}$ and *Hira*$^{fl/fl}$ embryos, as well as 100 adult HSCs from the bone marrow of *Mx1-Cre; Hira*$^{fl/fl}$ and *Hira*$^{fl/fl}$ mice 7 days after poly(I:C) treatment and transplanted them into lethally irradiated mice (Figure 2F). Transplantation of *Hira*-deficient HSCs derived from either fetal liver or adult bone marrow resulted in low granulocytic-monocytic, but no lymphoid, reconstitution at the earliest time point analyzed, which became undetectable at later time points (Figure 2G). *Hira*-deficient HSCs were depleted 16 weeks after transplantation (Figure S2J). These results demonstrate that, while *Hira* deletion is compatible with clonogenicity of HSCs *in vitro*, *Hira* is essential for HSCs to regenerate the hematopoietic system upon transplantation.

To assess the early contributions of *Hira*-deleted HSCs toward red blood cells and platelets, we performed a similar HSC competitive transplant assay with 100 HSCs sorted from the bone marrow of *Ubc-GFP; Mx1-Cre; Hira*$^{fl/fl}$ and control *Ubc-GFP; Hira*$^{fl/fl}$ mice 7 days after poly(I:C) (Figure S2K). In contrast to the diminished granulocytic-monocytic and lymphoid reconstitution by *Mx1-Cre; Hira*$^{fl/fl}$ HSCs (Figure 2G), red blood cells and platelets exhibited robust regeneration by *Hira*-deficient HSCs indistinguishable from that of wild-type HSCs (Figure 2H). By analyzing

(H) Donor-derived chimerism, as assessed by GFP positivity, within RBC and platelets (PLT) from transplanted HSCs isolated from *Ubc-GFP; Hira*$^{fl/fl}$ (WT) or *Ubc-GFP; Mx1-Cre; Hira*$^{fl/fl}$ (KO) mice (n = 3–5 mice).

(I and J) A representative flow cytometry plot (I) and quantification (J) of the five fractions of erythroid progenitors expressing CD71 and/or Ter119 in the GFP^{+} BM cells 8 weeks post-transplantation (n = 3–4 mice).

(K) Frequency of CD71^{+} erythroid cells after sorting HSCs into culture (n = 3 mice).

All data represent the mean ± standard deviation; *p < 0.05, **p < 0.01, and ***p < 0.001 by Student's t test.

See also Figure S2.

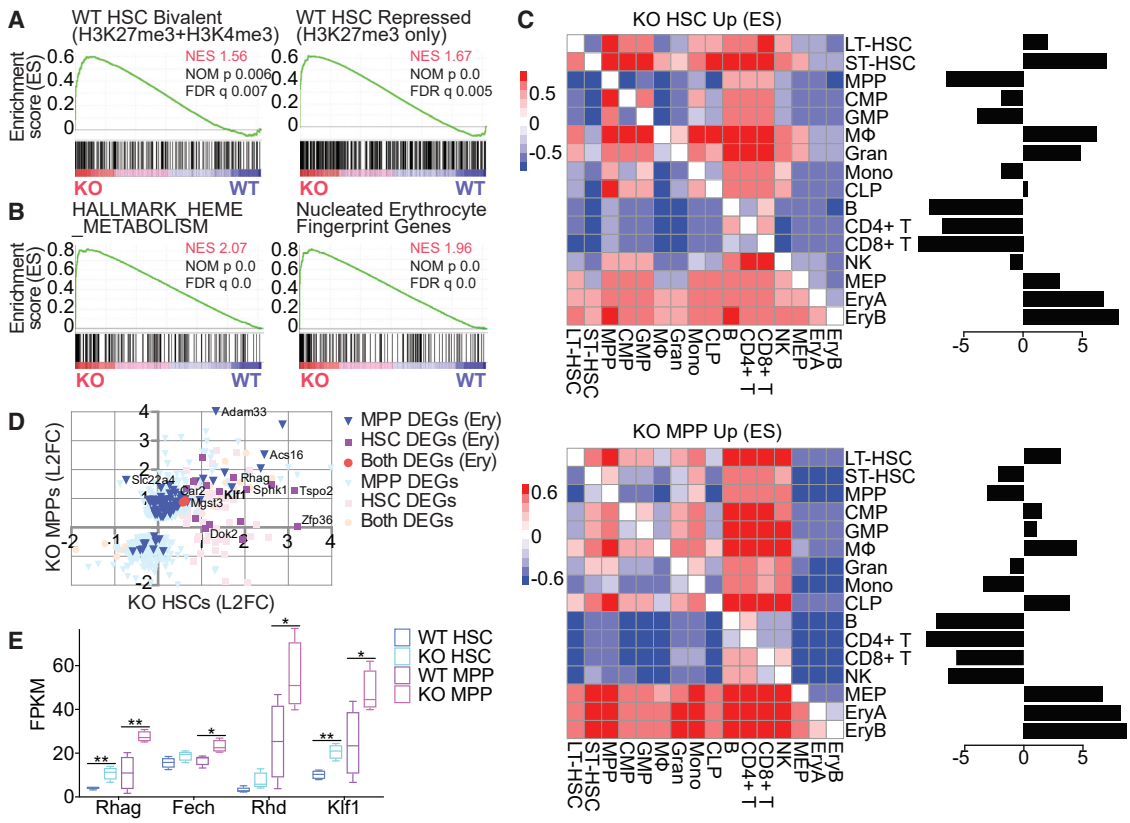

Figure 3. *Hira* loss increases erythroid gene expression in HSCs

(A and B) GSEA of RNA-seq data from WT (*Hira*$^{fl/fl}$) and KO (*Mx1-Cre; Hira*$^{fl/fl}$) HSCs for PRC2 target genes that are bivalent (H3K27me3 and H3K4me3) or repressed (H3K27me3 only) (A) and heme metabolism hallmark gene set or genes expressed in nucleated erythrocytes (B). (C) Pairwise GSEAs assessing enrichment of genes that are upregulated in KO HSCs (top) or MPPs (bottom) in different hematopoietic cell types in a pairwise manner. The cumulative enrichment score of the gene sets for each hematopoietic cell type is shown (right). (D) Scatterplot of $\log_2$(fold change) (L2FC) for erythroid differentially expressed genes (DEGs) (Ery) in HSCs, MPPs, or both (WT versus KO). (E) Expression of *Rhag*, *Fech*, *Rhd*, and *Klf1* as determined by fragments per kilobase of transcript per million (FPKM) values. All data represent the mean ± standard deviation; *p < 0.05 and **p < 0.01 by Student's t test.
See also Figure S3.

recipient bone marrow cells at 8 weeks post-transplantation, we also determined that *Hira*-deleted HSCs had increased differentiation into MEPs and CD71^{+}Ter119^{Low} early erythroid progenitors (Figures 2I, 2J, and S2L). In addition, *Hira*-deleted HSCs showed increased differentiation into CD71^{+} erythroid cells compared with wild-type HSCs (Figure 2K). Thus, while *Hira* deletion in HSCs significantly impaired granulocytic-monocytic and lymphoid reconstitution potential, the erythroid and thrombocytic lineages remained intact.

Hira loss increases erythroid gene expression in HSCs

To determine the role of *Hira* in adult HSC maintenance, we profiled the transcriptomes of HSCs and MPPs from adult *Mx1-Cre; Hira*$^{fl/fl}$ and *Hira*$^{fl/fl}$ mice 1 week after poly(I:C) treatment with RNA sequencing (RNA-seq) (Figures S3A and S3B). Gene set enrichment analysis (GSEA) revealed that PRC2 target genes were highly enriched in *Hira*-deficient HSCs (Figure S3C). This finding is consistent with the previous reports demonstrating that HIRA regulates PRC2-mediated repression of bivalent genes in embryonic stem cells (ESCs) (Banaszynski et al., 2013), but is nonetheless striking since the gene sets contained genes repressed by PRC2 in non-hematopoietic ESCs or fibroblasts.

To specifically investigate whether *Hira* is involved in PRC2-mediated gene repression in HSCs, we used two gene sets containing genes in HSCs marked by H3K27me3, a repressive mark deposited by the PRC2, or both H3K27me3 and H3K4me3, which defines bivalent genes (Mochizuki-Kashio et al., 2015; Sun et al., 2014) (Figures 3A and S3D). Both of these gene sets showed significant enrichment in *Hira*-deficient HSCs, indicating that

Hira deletion derepresses genes that are repressed or maintained in the bivalent state by the PRC2 complex.

In addition, we found that the most enriched hallmark gene set in *Hira*-deficient HSCs and MPPs was a heme metabolism gene set that includes genes involved in red blood cell biology, such as *Rhag*, *Fech*, *Rhd*, and *Klf1* (Figures 3B–3E). The finding that *Hira* deletion increased the expression of erythroid gene expression in HSCs and MPPs prompted us to comprehensively examine whether *Hira* deletion induces lineage-specific gene signatures. We thus performed a pairwise GSEA (Viny et al., 2015) to assess the enrichment of gene signatures associated with *Hira*-deficient HSCs or MPPs in 16 hematopoietic cell populations (Figure 3C). We found that myeloid and erythroid cells were enriched for the gene signatures induced after *Hira* deletion, suggesting that *Hira*-deficient HSCs and MPPs exhibit myeloid and erythroid gene programs. GSEA using gene sets curated from genes uniquely expressed in each hematopoietic lineage (hematopoietic fingerprint; Chambers et al., 2007) also showed that *Hira*-deficient HSCs are enriched for the nucleated erythrocyte gene signature (Figure 3B). In addition, a subset of bivalent and erythroid genes had increased expression in both HSCs and MPPs after *Hira* deletion, and genes with increased expression in *Hira*-deficient HSCs were enriched for GATA2 and GATA1 motifs in their promoters (Figures 3D, 3E, S3D, and S3E). These transcriptome changes suggest that *Hira*-deficient HSCs have increased differentiation toward the erythroid lineage.

Cell division exacerbates the derepression of erythroid genes in *Hira*-deficient HSCs

Since HIRA deposits H3.3 independent of DNA replication, we hypothesized that cell division in the absence of *Hira* would accelerate the histone H3 disequilibrium due to deposition of DNA replication-dependent histone H3.1 and H3.2, which may lead to more significant changes in gene expression. To address this hypothesis, we crossed the *Mx1-Cre; Hira*$^{fl/fl}$ mice with *Rosa26-M2rtTA; TetOP-H2B-GFP* mice (Foudi et al., 2008; Wilson et al., 2008) to enable expression of H2B-GFP upon doxycycline administration.

We treated *Mx1-Cre; Hira*$^{fl/fl}$*; Rosa26-M2rtTA; TetOP-H2B-GFP* and *Hira*$^{fl/fl}$*; Rosa26-M2rtTA; TetOP-H2B-GFP* with doxycycline for 6 weeks and then with poly(I:C) to delete *Hira*. Fifteen days after the last poly (I:C) injection we analyzed GFP intensity in HSCs and MPPs (Figure 4A). As reported previously (Foudi et al., 2008; Nakada et al., 2014; Wilson et al., 2008), quiescent HSCs and MPPs retained high GFP intensity compared with rapidly dividing LK and lineage$^-$ cells (Figure S4A). Although deletion of *Hira* did not affect the overall frequencies of GFP$^+$ HSCs or MPPs (Figure S4A), we detected lower frequencies of *Hira*-deficient GFP^{low} HSCs/MPPs relative to GFP^{high} *Hira*-deficient HSCs/MPPs (Figures 4B and 4C). These results suggest either that *Hira* deletion delays cell division of HSCs/MPPs or that HSCs/MPPs that have divided (GFP^{low} HSCs/MPPs) undergo apoptosis or differentiation. Given that we have detected no differences in cell division rates or apoptosis of HSCs/MPPs after *Hira* deletion (Figures S2A and S2B), we postulated that *Hira*-deficient HSCs/MPPs are prone to differentiation after cell division.

To address this possibility, we performed RNA-seq of H2B-GFP high and low HSCs and MPPs with or without *Hira* deletion (Figure 4D). Gene ontology (GO) analysis of the differentially expressed genes showed that the most significant changes occurred in the GFP^{low} HSC fraction after *Hira* deletion. Specifically, gene signatures associated with myeloid and erythroid differentiation showed significant upregulation in *Hira*-deficient GFP^{low} HSCs and MPPs (Figures 4E and S4F). Conversely, downregulated genes in *Hira*-deleted GFP^{low} HSCs were mostly associated with B and T cell lineages (Figure S4F). Unsupervised hierarchical clustering of the differentially expressed genes associated with *Hira* deletion revealed that similar transcriptional changes occur in *Hira*-deficient HSCs and MPPs upon division (Figure S4D). Interestingly, this cluster of upregulated genes in GFP^{low} *Hira*-deficient HSCs/MPPs was enriched for erythropoiesis-related genes, including key erythroid transcription factors *Gata1* and *Klf1*, hemoglobin genes *Hba-a1* and *Hbb-b1*, and erythroid antigens *Rhag* and *Rhd* (Figure S4D).

GO analysis of genes differentially expressed in GFP^{low} cells compared with GFP^{high} cells showed upregulation of cell division gene signature in both wild-type and *Hira*-deficient HSPCs (Figure S4E). Interestingly, more bivalent genes and erythrocyte fingerprint genes exhibited increased expression in *Hira*-deficient HSCs and MPPs after cell division compared with wild-type HSCs (Figures 4F–4H and S4E). In contrast, long-term HSC (LT-HSC) fingerprint genes showed decreased expression after cell division in *Hira*-deficient HSCs and MPPs more so than in wild-type HSCs and MPPs (Figure 4I). These results show that cell division after *Hira* deletion increases the expression of bivalent and erythroid differentiation genes while reducing LT-HSC gene expression.

Hira loss increases DNA accessibility and decreases histone H3.3 at hematopoietic transcription factor motifs

To determine how HIRA regulates the expression of bivalent and erythroid genes, we performed assay for transposase-accessible chromatin with high-throughput sequencing (ATAC-seq) and H3.3 chromatin immunoprecipitation sequencing (ChIP-seq) in *Hira*-deficient HSCs 1 week after deletion. Differential peak analysis of the ATAC-seq profile revealed 424 differential peaks in *Hira*-deleted HSCs and 401 differential peaks in wild-type HSCs. Most differential

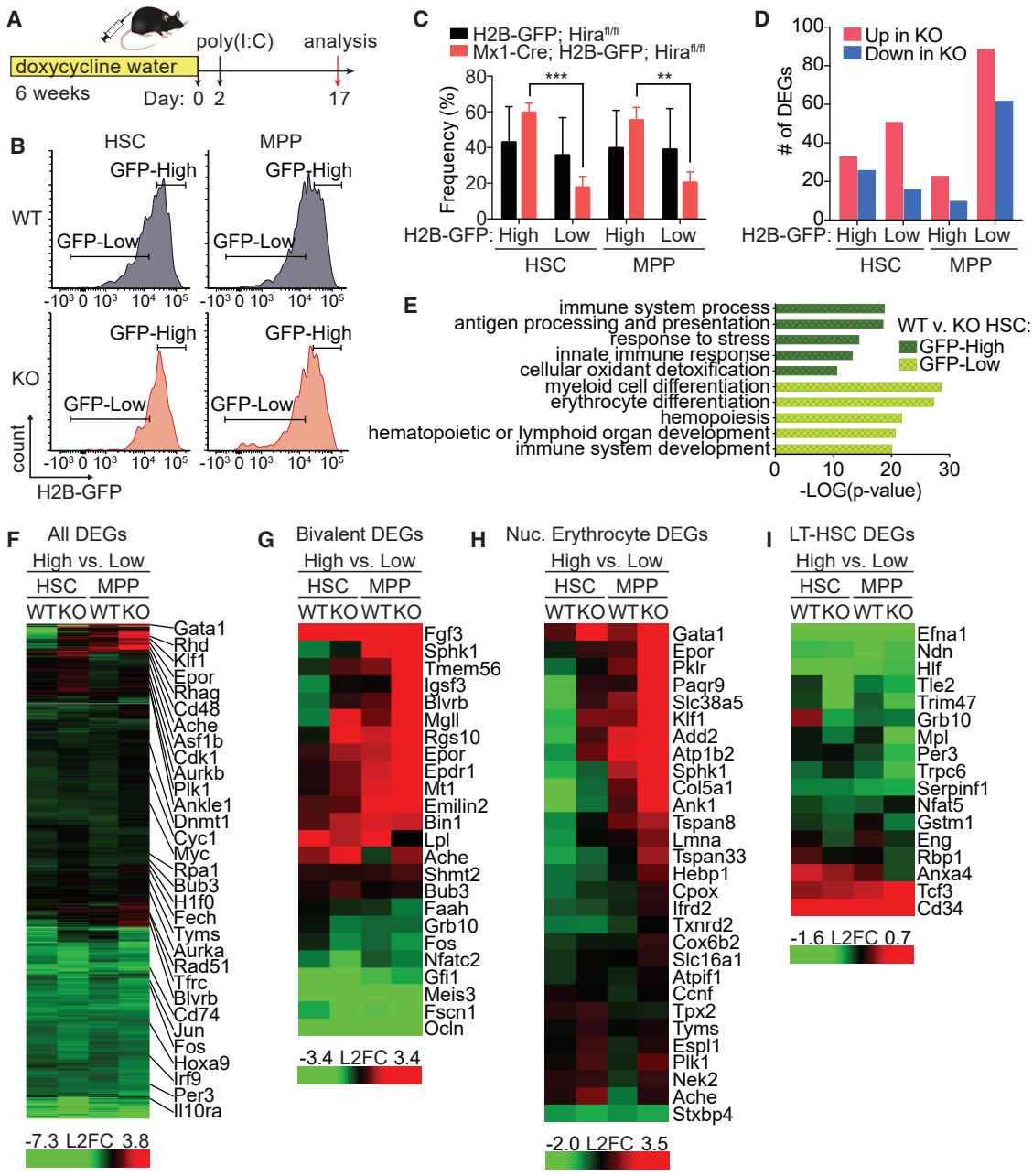

Figure 4. Cell division exacerbates the derepression of erythroid genes in *Hira*-deficient HSCs

(A) Diagram showing treatment of *Rosa26-M2rtTA; TetOP-H2B-GFP; Hira$^{fl/fl}$* mice with or without *Mx1-Cre* to pulse-chase H2B-GFP labeling with doxycycline and delete *Hira* with poly(I:C).

(B) Flow plots showing the gating used to separate H2B-GFP high/low fractions (n = 3 mice).

(C) Frequencies of H2B-GFP high/low HSCs/MPPs in WT and KO mice (n = 3 mice).

(D) The number of DEGs (WT versus KO) that are upregulated or downregulated between H2B-GFP high and low cells.

(E) GO terms significantly enriched in WT versus KO HSCs that are either H2B-GFP high or low.

(F–I) Unsupervised clustering of all DEGs (F), bivalent DEGs (G), nucleated erythrocyte DEGs (H), and DEGs associated with LT-HSCs (I) for H2B-GFP high/low cells.

All data represent the mean ± standard deviation; **p < 0.01, and ***p < 0.001 by Student's t test.

See also Figure S4.

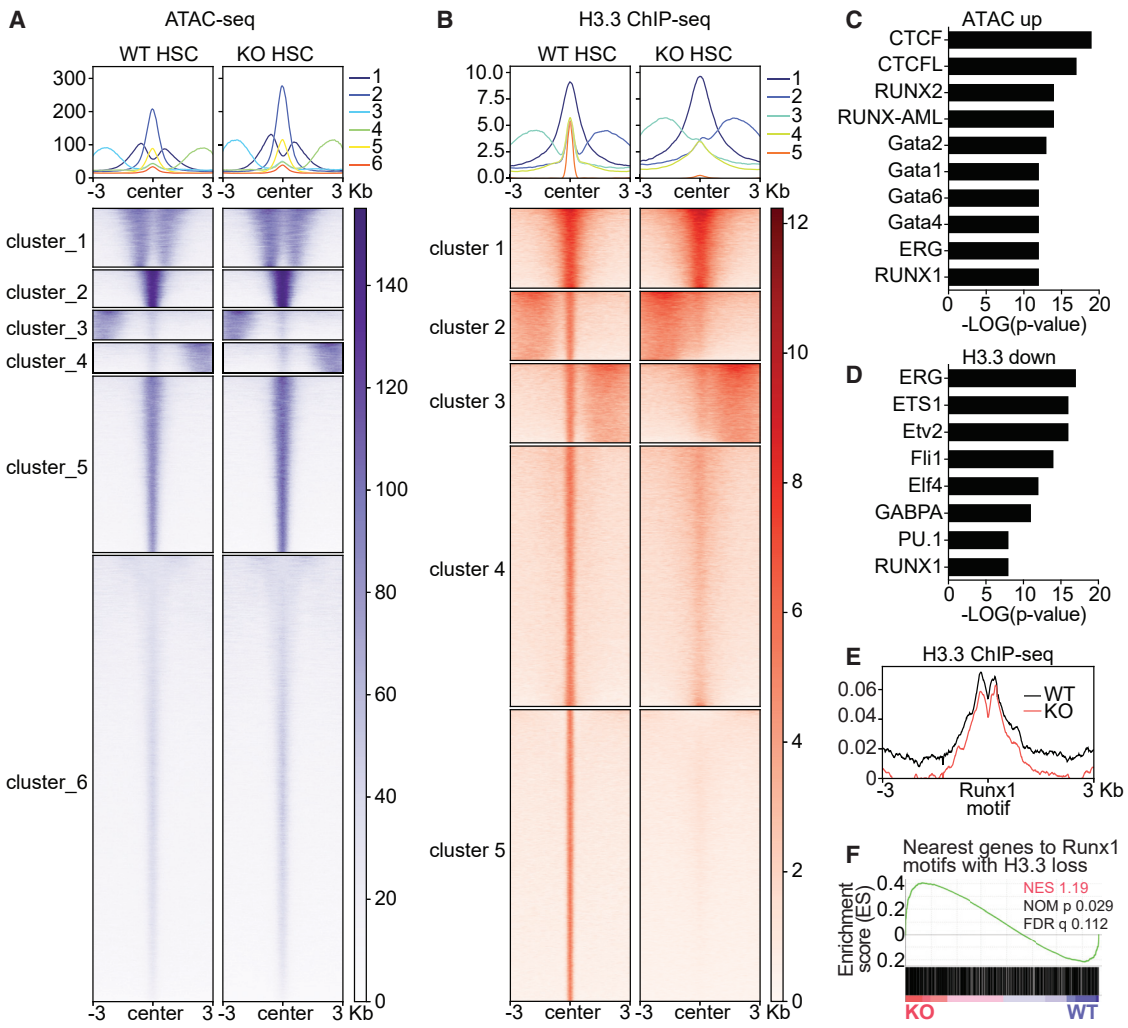

Figure 5. *Hira* loss increased DNA accessibility and decreased histone H3.3 at hematopoietic transcription factor motifs

(A and B) Heatmaps and profile plots of ATAC-seq (A) and H3.3 ChIP-seq (B) data from WT and KO HSCs with six clusters of peaks identified by k-means clustering.

(C and D) Motif enrichment analysis in differential ATAC-seq peaks called in KO versus WT HSCs (ATAC up, C) or in differential H3.3 ChIP-seq peaks called in WT versus KO HSCs (H3.3 down, D).

(E) Genome-wide H3.3 ChIP-seq profile plot at RUNX1 motifs.

(F) GSEA shows that genes in close proximity to RUNX1 motifs with reduced H3.3 binding in KO HSCs are derepressed.

ATAC-seq peaks were located within introns, promoters, and intergenic DNA (Figure S5A).

To better understand these changes in DNA accessibility we performed k-means clustering of the ATAC-seq peaks called in wild-type HSCs. Among the six clusters exhibiting different patterns of accessibility, cluster 2 contained the most accessible DNA in wild-type HSCs and showed the largest increase in accessibility after *Hira* deletion (Figure 5A). Other ATAC-seq peak clusters also exhibited varying degrees of increased accessibility in *Hira*-depleted HSCs, demonstrating a general requirement for HIRA in restricting DNA accessibility.

We then performed ChIP-seq profiling for endogenous histone H3.3 using an antibody that recognizes H3.3 specifically and efficiently (Figures S5B and S5C). We found 48,193 differential H3.3 peaks in wild-type HSCs versus 37,205 differential peaks in *Hira*-deleted HSCs. Most of the differential H3.3 peaks in wild-type and *Hira*-deficient HSCs were located within introns and intergenic DNA in addition to retrotransposon DNA (Figure S5A). k-means clustering identified five distinct clusters of H3.3 binding peaks in wild-type HSCs (Figure 5B). Clusters 1, 2, and 3 gained H3.3 binding after *Hira* deletion, whereas clusters 4 and 5 lost H3.3 after *Hira* deletion. These results suggest

that HIRA maintains appropriate H3.3 positioning at certain loci in HSCs.

Motif enrichment analysis of the differential peaks identified in both our ATAC-seq and our H3.3 ChIP-seq experiments revealed that ERG and RUNX1 motifs are enriched in regions of increased accessibility and reduced H3.3 occupancy in *Hira*-deleted HSCs (Figures 5C and 5D). We also observed an enrichment of CTCF motifs and GATA family motifs in peaks with increased DNA accessibility after *Hira* loss (Figure 5C). These findings are consistent with prior studies reporting that HIRA directly interacts with both CTCF and RUNX1 (Majumder et al., 2015; Pchelintsev et al., 2013). The increase in accessibility at GATA1 motifs is also consistent with the observed increase in erythroid differentiation genes with GATA1 motifs in their promoter.

To study the relationship between H3.3 dysregulation and DNA accessibility at transcription factor motifs in *Hira*-deficient HSCs, we then assessed chromatin accessibility and H3.3 occupancy at RUNX1, ERG, and PU.1 motifs genome wide (Figures 5E and S5D–S5F). This showed that RUNX1 motifs have a noticeable loss of H3.3 after *Hira* deletion (Figure S5F). To assess whether H3.3 loss at RUNX1 motifs affects gene expression, we performed GSEA on the genes nearest to H3.3 peaks with RUNX1 motifs that had reduced H3.3 signals in *Hira*-deleted HSCs (Figure 5G). The expression of these genes was significantly increased in *Hira*-deficient HSCs, suggesting that HIRA-mediated H3.3 deposition at RUNX1 motifs represses gene expression in HSCs. GO analysis determined that these genes adjacent to H3.3-reduced RUNX1 motifs were involved in developmental processes, such as cell differentiation, hemopoiesis, and cell fate commitment (Figure S5H). These results suggest that *Hira* restricts DNA accessibility at hematopoietic transcription factor binding sites in HSCs.

H3.3 occupies a subset of polycomb-repressed genes in a *Hira*-dependent manner

To understand how HIRA maintains appropriate HSC chromatin states, we compared the differential peaks from our H3.3 ChIP-seq data in wild-type and *Hira*-deleted HSCs with our ATAC-seq data. Most H3.3 depletion after *Hira* deletion occurred in regions of low DNA accessibility, whereas regions with increased H3.3 were mostly found in highly accessible DNA (Figure 6A). These results suggest that HIRA preferentially maintains H3.3 in regions of low chromatin accessibility.

We next examined whether H3.3 occupancy further separates chromatin states defined by multiple histone modifications in HSCs. We used ChromHMM (Ernst and Kellis, 2012) with published histone H3 modification and our H3.3 ChIP-seq datasets and identified 18 distinct chromatin states that were defined by the presence or absence of H3.3 (Figure 6B). From this 18-state analysis, we found that all of the chromatin states associated with active gene expression existed in both H3.3+ and H3.3− states (Figure 6B). These included states with histone marks typically associated with enhancers (states 1 and 2), active promoters (states 3 and 4), active transcription start sites (TSSs) (states 5 and 6), and strong transcription (states 7 and 8). The one exception to this dichotomy of active chromatin states defined by H3.3 was the weak enhancer chromatin state (state 16) that is only slightly enriched with enhancer-associated histone marks, which existed solely as an H3.3+ state. The polycomb-repressed chromatin state was also separated into H3.3+ and H3.3− states (states 10 and 11). In contrast, the bivalent promoter chromatin state (state 9) was exclusively H3.3+. Altogether, these chromatin-state analyses reveal a novel paradigm of HSC chromatin states in which the presence or absence of histone variant H3.3 defines a subset of active and polycomb-repressed chromatin states and highlights the association of H3.3 with bivalent promoters and polycomb-repressed chromatin in HSCs.

We then assessed the enrichment of the each state in superenhancers (Khan and Zhang, 2016) and TSS. The H3.3+ enhancer state (state 1) was the most highly enriched state in superenhancers and was 2.5× more enriched in superenhancers than the H3.3− enhancer state (state 2), despite covering a smaller portion of the genome (Figures 6C and S6A). We also found that the H3.3+ bivalent promoter state was highly enriched in TSSs and CpG islands (Figures 6C and S6B). In contrast, the H3.3− polycomb-repressed state was not highly enriched in any of these regions, despite comprising approximately 20% of the genome. These results validate our chromatin-state analysis and show a functional difference in gene regulation between H3.3-marked chromatin states based on their associated histone marks. Our findings on H3.3+ chromatin states associated with superenhancers and CpG islands also demonstrate that the epigenetic status of gene regulatory elements in HSCs can be better resolved through chromatin-state modeling that includes information about H3.3 binding in HSCs.

To identify which chromatin states are affected by *Hira* deletion, we then compared this model with our transcriptomic and epigenetic profiling of *Hira*-deleted HSCs. GSEA showed that H3.3+ bivalent promoter and H3.3+ polycomb-repressed genes are significantly derepressed, but that the H3.3− polycomb-repressed genes are not (Figures 6D, 6E, S6C, and S6D). These H3.3+ PRC2-target genes are enriched in development and cell fate determination genes, whereas the H3.3− polycomb-repressed genes are enriched in non-developmental genes (Figure 6F). Interestingly, while both the H3.3+ bivalent promoter and the H3.3+ polycomb-repressed states increased accessibility in

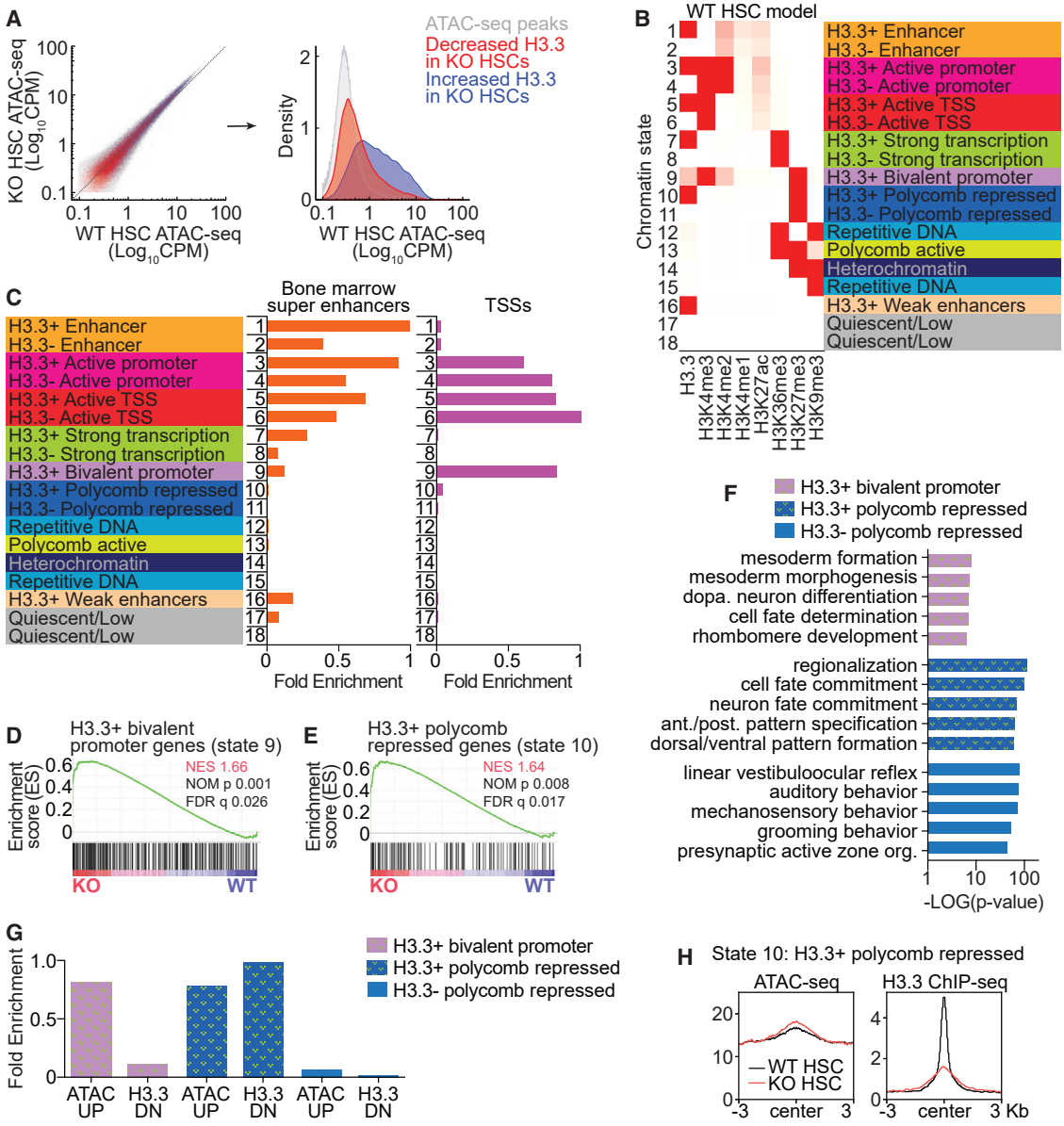

Figure 6. H3.3 occupies a subset of polycomb-repressed genes in a *Hira*-dependent manner

(A) Scatterplot correlating DNA accessibility in WT and *Hira* KO HSCs using ATAC-seq signals with overlapping H3.3 peaks that decreased (red) or increased (blue) in KO HSCs. The gray histogram shows ATAC-seq peaks not overlapping any H3.3 differential peaks.

(B) ChromHMM emission parameters for an 18-chromatin-state model of HSCs with dark red indicating a high probability of each histone mark being found in each chromatin state (left). Each state is labeled based on the regulatory elements associated with their corresponding histone marks (right).

(C) The fold enrichment of each WT HSC chromatin state overlapping bone marrow superenhancers and TSSs normalized to the maximum enrichment of each region for all chromatin states (range = 0–1).

(D and E) GSEAs show that KO HSCs have derepression of genes with promoters or TSSs overlapping states 9 (D) or 10 (E).

(F) Selected GO terms significantly associated with genes with promoter or TSS regions overlapping state 9, 10, or 11.

(G) The fold enrichment of state 9, 10, or 11 within regions where ATAC-seq signals are increased (ATAC UP) or H3.3 is reduced (H3.3 DN) in KO HSCs normalized to the maximum enrichment of each region for all chromatin states (range = 0–1).

(H) Profile plots of ATAC-seq and H3.3 ChIP-seq data at the H3.3+ polycomb repressed (state 10) chromatin state in WT and *Hira* KO HSCs.

Hira-deleted HSCs, only the H3.3+ polycomb-repressed state reduced H3.3 binding upon *Hira* deletion (Figures 6G, 6H, and S6E). Altogether, these results establish that HIRA is essential for the continued repression of developmental genes with regulatory regions marked with both H3.3 and H3K27me3 in HSCs.

DISCUSSION

Our study shows that the regulation of histone variant H3.3 by HIRA is essential for the maintenance of adult HSCs. We establish that bivalent promoters and a subset of polycomb-repressed chromatin are defined by H3.3 occupancy, and repression of genes associated with these chromatin states requires HIRA. Importantly, polycomb-repressed chromatin bound by H3.3 depends on HIRA to maintain H3.3 occupancy and its inaccessible configuration. We also find that *Hira* is particularly important for repressing differentiation-associated genes in HSCs upon cell division. Our study extends prior studies demonstrating that HIRA-mediated H3.3 incorporation is important for non-dividing cells, by establishing the essentiality of *Hira* in quiescent adult HSCs to prevent precocious differentiation.

We demonstrate that *Hira* is essential for the maintenance of postnatal and adult bone marrow HSCs but not committed progenitor cells. In contrast, *Hira*-deleted fetal liver HSCs were able to expand and home to the bone marrow at the time of birth. However, fetal liver HSCs exhibited little reconstitution capacity upon transplantation, and they became depleted within weeks after migrating to the bone marrow. These results suggest that HIRA is required to adapt to the bone marrow environment or to stresses present during transplantation. Both fetal liver HSCs and committed progenitor cells divide rapidly, while adult HSCs divide much more rarely. Other non-dividing cell types, such as post-mitotic neurons, oocytes, and muscle stem cells, have also been shown to rely on HIRA for cell-type-specific gene expression and differentiation (Maze et al., 2014, 2015; Nashun et al., 2015). Our study demonstrates that adult HSCs that rarely divide are also highly dependent upon *Hira*.

A recent paper showed that *Hira* loss underlies immune cell deficiencies in DiGeorge syndrome patients by impairing HSPC differentiation (Chen et al., 2020). Consistently, our HSC transplantation assays showed that *Hira* deletion severely compromised myeloid and lymphoid lineage reconstitution. In contrast, erythroid lineage reconstitution by *Hira*-deficient HSCs was indistinguishable from that of wild-type HSCs. Changes in HSC differentiation potential were accompanied by increased erythroid gene expression, establishing that HSCs depend on HIRA to repress erythroid-lineage genes. We also discovered that HIRA is required to suppress expression of PRC2 target genes in adult HSCs and MPPs. The finding that adult but not fetal liver HSCs depend on HIRA is also reminiscent of the differential dependence of HSCs on the PRC2 component EED (Xie et al., 2014). Our gene expression and chromatin-state analyses corroborate these genetic analyses to demonstrate the cooperation of HIRA with the PRC2 complex.

We found that increased bivalent and erythroid gene expression is exacerbated in *Hira*-deleted HSCs after cell division. HSC self-renewal capacity is progressively deteriorated by successive rounds of cell division (Bernitz et al., 2016; Foudi et al., 2008; Wilson et al., 2008). Our study extends these reports by establishing that a *Hira*-dependent mechanism ensures repression of erythroid gene expression in order to prevent differentiation as HSCs divide. Further lineage tracing experiments are needed to fully elucidate the fate of HSCs that have undergone division in the absence of *Hira*.

Our H3.3 profiling in HSCs provides a novel means to further segregate active and polycomb-repressed chromatin states. While active and polycomb-repressed chromatin had both H3.3+ and H3.3− states, the bivalent promoter chromatin state existed only as an H3.3+ state. H3.3 deposition at bivalent promoters was not dependent on *Hira*, although *Hira* deletion led to increased gene expression, demonstrating that HIRA represses bivalent promoters independent of H3.3 deposition. This may be due to HIRA-dependent recruitment of PRC2 to target genes and HIRA-independent deposition of H3.3, both of which have been observed in ESCs (Banaszynski et al., 2013; Goldberg et al., 2010). In this scenario, *Hira* deletion does not necessarily lead to loss of H3.3 due to yet unknown factors that deposit H3.3 independent of HIRA, but leads to failed recruitment of PRC2 and loss of repressive H3K27me3 on HIRA target genes, leading to derepression of bivalent genes while retaining H3.3. The polycomb-repressed chromatin existed as both H3.3+ and H3.3− states. H3.3+, but not H3.3−, polycomb-repressed chromatin became more accessible, lost H3.3 occupancy, and became derepressed upon *Hira* deletion. Thus, maintenance of gene repression by HIRA is linked to H3.3 deposition in polycomb-repressed chromatin. Our study provides a new layer of resolution to our understanding of chromatin states in HSCs and reveals dichotomous polycomb-repressed states distinguished by HIRA-H3.3 dependence.

EXPERIMENTAL PROCEDURES

Mouse strains

Mice were housed in AAALAC-accredited, specific-pathogen-free animal care facilities at Baylor College of

Medicine (BCM) with 12-h light-dark cycle and received standard chow *ad libitum*. All procedures were approved by the BCM (protocol AN-5858) Institutional Animal Care and Use Committees. *Hira* mutant mice (*Hira*$^{tm1a(EUCOMM)Wtsi/+}$) were crossed with FLPe mice to remove selection markers flanked by FRT sites. The resulting mice (*Hira*$^{fl/+}$) were crossed with *Vav1-iCre* (JAX 008610) (Georgiades et al., 2002) or *Mx1-Cre* (JAX 005673) (Kuhn et al., 1995) mice. The *Mx1-Cre; Hira*$^{fl/fl}$ mice were also bred to *R26-loxP-stop-loxP-EYFP* (JAX 006148) (Srinivas et al., 2001), *Ubc-GFP* (JAX 004353) (Schaefer et al., 2001), or *Rosa26-M2rtTA; TetOP-H2B-GFP* (JAX 016836) (Foudi et al., 2008) mice on a C57BL/6 background. Both male and female mice were used in these studies, and all experimental units were age matched.

RNA-seq

HSCs and MPPs were sorted into Trizol and RNA purified according to the manufacturer's instructions. DNase I-treated RNA samples were purified, and cDNA was synthesized and amplified with a SMART-Seq2 protocol. The cDNA was then fragmented and bar-coded for sequencing using a Nextera XT kit. RNA-seq libraries were sequenced on an Illumina Sequencer (Illumina, San Diego, CA). Reads were mapped to mm10 using STAR (version 2.5.2b; Dobin and Gingeras, 2016) and analyzed using DESeq2 (version 1.12.4; Love et al., 2014). The principal-component analysis plot was generated with deepTools.

ATAC-seq

ATAC-seq was performed essentially as described (Buenrostro et al., 2013). Five thousand HSCs were tagmented with 0.5 μL of Tn5 (0.885 mg/mL) and incubated at 37°C for 30 min. Tagmented DNA, purified by a ZYMO DNA purification kit, was PCR amplified with NEBNext Q5 Hot Start HiFi PCR Master Mix (NEB M0543S). The library was purified using SPRI beads and sequenced on the Illumina HiSeq 2000 platform. Reads were mapped to mm10 using Bowtie2, and peaks were called on each sample individually using MACS2. Differential peaks were obtained on overlapping peaks using PePr. Heatmaps were generated using the deepTools computeMatrix algorithm whereby the center of each location (from the BED file) was used as the reference point and was extended ±3 kb from the center point.

ChIP-seq

Low-cell-number ChIP-seq (5,000 HSCs) was performed, as described previously, with a native ChIP-seq protocol (Hu et al., 2019). MNase-digested samples were used for ChIP with anti-H3.3 antibodies (MABE872, Millipore). The input and immunoprecipitated DNA was cleaned using SPRI beads, and the NEBNext Ultra II kit was used to generate bar-coded libraries for Illumina sequencing. Reads were mapped to mm10 with Bowtie, peaks were called using both PePr and MACS2, and deepTools was used to generate all heatmaps.

Resources

All key resources used in this study are listed in Table S1.

Data and code availability

The sequencing dataset generated in this study is in the Gene Expression Omnibus under accession no. GEO: GSE163052.

SUPPLEMENTAL INFORMATION

Supplemental information can be found online at https://doi.org/10.1016/j.stemcr.2021.06.009.

AUTHOR CONTRIBUTIONS

Conceptualization, R.L.M and D.N.; methodology, R.L.M., M.V.H., M.C.H., N.L.Y., and D.N.; software, K.A.H.; investigation, R.L.M., K.A.H., A.K., M.V.H., M.C.H., X.S., J.T., R.C., T.H., Y.T., and A.L.; writing – original draft, R.L.M. and D.N.; writing – review & editing, R.L.M. and D.N.; funding acquisition, R.L.M. and D.N.; resources, J.F.M., N.L.Y., and D.N.; project administration, D.N.

DECLARATION OF INTERESTS

J.F.M. is a founder of and owns shares in Yap Therapeutics. The other authors report no conflicts.

ACKNOWLEDGMENTS

This work was supported by the National Institutes of Health (R01CA193235 and R01DK107413 to D.N.; F31DK112542 to R.L.M.; R01GM139295 to N.L.Y.; HL127717, HL130804, and HL118761 to J.F.M.; and F31HL136065 to M.C.H.). X.S. and D.N. are a Special Fellow and a Scholar of the Leukemia and Lymphoma Society, respectively. T.H. was supported by a training grant from CPRIT (RP160283). J.F.M. was also supported by the Vivian L. Smith Foundation, State of Texas funding, and Fondation LeDucq Transatlantic Networks of Excellence in Cardiovascular Research (14CVD01) "Defining the genomic topology of atrial fibrillation." Flow cytometry was partially supported by the NIH (S10RR024574, AI036211, P30CA125123). Sequencing was partially supported by the NIH (P30CA125123).

Received: January 16, 2021
Revised: June 11, 2021
Accepted: June 11, 2021
Published: July 8, 2021

REFERENCES

Banaszynski, L.A., Wen, D., Dewell, S., Whitcomb, S.J., Lin, M., Diaz, N., Elsasser, S.J., Chapgier, A., Goldberg, A.D., Canaani, E., et al. (2013). Hira-dependent histone H3.3 deposition facilitates PRC2 recruitment at developmental loci in ES cells. Cell *155*, 107–120.

Bernitz, J.M., Kim, H.S., MacArthur, B., Sieburg, H., and Moore, K. (2016). Hematopoietic stem cells count and remember self-renewal divisions. Cell *167*, 1296–1309 e1210.

Buenrostro, J.D., Giresi, P.G., Zaba, L.C., Chang, H.Y., and Greenleaf, W.J. (2013). Transposition of native chromatin for fast and sensitive epigenomic profiling of open chromatin, DNA-binding proteins and nucleosome position. Nat. Methods *10*, 1213–1218.

Burgess, R.J., and Zhang, Z. (2013). Histone chaperones in nucleosome assembly and human disease. Nat. Struct. Mol. Biol. *20*, 14–22.

Challen, G.A., Sun, D., Jeong, M., Luo, M., Jelinek, J., Berg, J.S., Bock, C., Vasanthakumar, A., Gu, H., Xi, Y., et al. (2011). Dnmt3a is essential for hematopoietic stem cell differentiation. Nat. Genet. *44*, 23–31.

Chambers, S.M., Boles, N.C., Lin, K.Y., Tierney, M.P., Bowman, T.V., Bradfute, S.B., Chen, A.J., Merchant, A.A., Sirin, O., Weksberg, D.C., et al. (2007). Hematopoietic fingerprints: an expression database of stem cells and their progeny. Cell Stem Cell *1*, 578–591.

Chen, C., Sun, M.A., Warzecha, C., Bachu, M., Dey, A., Wu, T., Adams, P.D., Macfarlan, T., Love, P., and Ozato, K. (2020). HIRA, a DiGeorge syndrome candidate gene, confers proper chromatin accessibility on HSCs and supports all stages of hematopoiesis. Cell Rep. *30*, 2136–2149 e2134.

Dobin, A., and Gingeras, T.R. (2016). Optimizing RNA-seq mapping with STAR. Methods Mol. Biol. *1415*, 245–262.

Elsasser, S.J., Noh, K.M., Diaz, N., Allis, C.D., and Banaszynski, L.A. (2015). Histone H3.3 is required for endogenous retroviral element silencing in embryonic stem cells. Nature *522*, 240–244.

Ernst, J., and Kellis, M. (2012). ChromHMM: automating chromatin-state discovery and characterization. Nat. Methods *9*, 215–216.

Foudi, A., Hochedlinger, K., Van Buren, D., Schindler, J.W., Jaenisch, R., Carey, V., and Hock, H. (2008). Analysis of histone 2B-GFP retention reveals slowly cycling hematopoietic stem cells. Nat. Biotechnol. *27*, 84–90.

Georgiades, P., Ogilvy, S., Duval, H., Licence, D.R., Charnock-Jones, D.S., Smith, S.K., and Print, C.G. (2002). VavCre transgenic mice: a tool for mutagenesis in hematopoietic and endothelial lineages. Genesis *34*, 251–256.

Goldberg, A.D., Banaszynski, L.A., Noh, K.M., Lewis, P.W., Elsaesser, S.J., Stadler, S., Dewell, S., Law, M., Guo, X., Li, X., et al. (2010). Distinct factors control histone variant H3.3 localization at specific genomic regions. Cell *140*, 678–691.

Hake, S.B., and Allis, C.D. (2006). Histone H3 variants and their potential role in indexing mammalian genomes: the "H3 barcode hypothesis. Proc. Natl. Acad. Sci. U S A *103*, 6428–6435.

Henikoff, S., and Smith, M.M. (2015). Histone variants and epigenetics. Cold Spring Harb. Perspect. Biol. *7*, a019364.

Hu, T., Morita, K., Hill, M.C., Jiang, Y., Kitano, A., Saito, Y., Wang, F., Mao, X., Hoegenauer, K.A., Morishita, K., et al. (2019). PRDM16s transforms megakaryocyte-erythroid progenitors into myeloid leukemia-initiating cells. Blood *134*, 614–625.

Khan, A., and Zhang, X. (2016). dbSUPER: a database of super-enhancers in mouse and human genome. Nucleic Acids Res. *44*, D164–D171.

Kiel, M.J., Yilmaz, O.H., Iwashita, T., Terhorst, C., and Morrison, S.J. (2005). SLAM family receptors distinguish hematopoietic stem and progenitor cells and reveal endothelial niches for stem cells. Cell *121*, 1109–1121.

Kuhn, R., Schwenk, F., Aguet, M., and Rajewsky, K. (1995). Inducible gene targeting in mice. Science *269*, 1427–1429.

Lara-Astiaso, D., Weiner, A., Lorenzo-Vivas, E., Zaretsky, I., Jaitin, D.A., David, E., Keren-Shaul, H., Mildner, A., Winter, D., Jung, S., et al. (2014). Immunogenetics. Chromatin state dynamics during blood formation. Science *345*, 943–949.

Laurenti, E., and Gottgens, B. (2018). From haematopoietic stem cells to complex differentiation landscapes. Nature *553*, 418–426.

Lessard, J., and Sauvageau, G. (2003). Bmi-1 determines the proliferative capacity of normal and leukaemic stem cells. Nature *423*, 255–260.

Love, M.I., Huber, W., and Anders, S. (2014). Moderated estimation of fold change and dispersion for RNA-seq data with DESeq2. Genome Biol. *15*, 550.

Majumder, A., Syed, K.M., Joseph, S., Scambler, P.J., and Dutta, D. (2015). Histone chaperone HIRA in regulation of transcription factor RUNX1. J. Biol. Chem. *290*, 13053–13063.

Martire, S., and Banaszynski, L.A. (2020). The roles of histone variants in fine-tuning chromatin organization and function. Nat. Rev. Mol. Cell Biol. *21*, 522–541.

Maze, I., Noh, K.M., Soshnev, A.A., and Allis, C.D. (2014). Every amino acid matters: essential contributions of histone variants to mammalian development and disease. Nat. Rev. Genet. *15*, 259–271.

Maze, I., Wenderski, W., Noh, K.M., Bagot, R.C., Tzavaras, N., Purushothaman, I., Elsasser, S.J., Guo, Y., Ionete, C., Hurd, Y.L., et al. (2015). Critical role of histone turnover in neuronal transcription and plasticity. Neuron *87*, 77–94.

Mochizuki-Kashio, M., Aoyama, K., Sashida, G., Oshima, M., Tomioka, T., Muto, T., Wang, C., and Iwama, A. (2015). Ezh2 loss in hematopoietic stem cells predisposes mice to develop heterogeneous malignancies in an Ezh1-dependent manner. Blood *126*, 1172–1183.

Mochizuki-Kashio, M., Mishima, Y., Miyagi, S., Negishi, M., Saraya, A., Konuma, T., Shinga, J., Koseki, H., and Iwama, A. (2011). Dependency on the polycomb gene Ezh2 distinguishes fetal from adult hematopoietic stem cells. Blood *118*, 6553–6561.

Nakada, D., Oguro, H., Levi, B.P., Ryan, N., Kitano, A., Saitoh, Y., Takeichi, M., Wendt, G.R., and Morrison, S.J. (2014). Oestrogen increases haematopoietic stem-cell self-renewal in females and during pregnancy. Nature *505*, 555–558.

Nashun, B., Hill, P.W., Smallwood, S.A., Dharmalingam, G., Amouroux, R., Clark, S.J., Sharma, V., Ndjetehe, E., Pelczar, P., Festenstein, R.J., et al. (2015). Continuous histone replacement by Hira is essential for normal transcriptional regulation and de novo DNA methylation during mouse oogenesis. Mol. Cell *60*, 611–625.

Oguro, H., Ding, L., and Morrison, S.J. (2013). SLAM family markers resolve functionally distinct subpopulations of hematopoietic stem cells and multipotent progenitors. Cell Stem Cell *13*, 102–116.

Park, D., Spencer, J.A., Koh, B.I., Kobayashi, T., Fujisaki, J., Clemens, T.L., Lin, C.P., Kronenberg, H.M., and Scadden, D.T. (2012). Endogenous bone marrow MSCs are dynamic, fate-restricted participants in bone maintenance and regeneration. Cell Stem Cell *10*, 259–272.

Park, I.K., Qian, D., Kiel, M., Becker, M.W., Pihalja, M., Weissman, I.L., Morrison, S.J., and Clarke, M.F. (2003). Bmi-1 is required for maintenance of adult self-renewing haematopoietic stem cells. Nature *423*, 302–305.

Pchelintsev, N.A., McBryan, T., Rai, T.S., VanTuyn, J., Ray-Gallet, D., Almouzni, G., and Adams, P.D. (2013). Placing the HIRA histone chaperone complex in the chromatin landscape. Cell Rep *3*, 1012–1019.

Pietras, E.M. (2017). Inflammation: a key regulator of hematopoietic stem cell fate in health and disease. Blood *130*, 1693–1698.

Ray-Gallet, D., Woolfe, A., Vassias, I., Pellentz, C., Lacoste, N., Puri, A., Schultz, D.C., Pchelintsev, N.A., Adams, P.D., Jansen, L.E., et al. (2011). Dynamics of histone H3 deposition in vivo reveal a nucleosome gap-filling mechanism for H3.3 to maintain chromatin integrity. Mol. Cell *44*, 928–941.

Rebel, V.I., Kung, A.L., Tanner, E.A., Yang, H., Bronson, R.T., and Livingston, D.M. (2002). Distinct roles for CREB-binding protein and p300 in hematopoietic stem cell self-renewal. Proc. Natl. Acad. Sci. U S A *99*, 14789–14794.

Sandberg, M.L., Sutton, S.E., Pletcher, M.T., Wiltshire, T., Tarantino, L.M., Hogenesch, J.B., and Cooke, M.P. (2005). c-Myb and p300 regulate hematopoietic stem cell proliferation and differentiation. Dev. Cell *8*, 153–166.

Schaefer, B.C., Schaefer, M.L., Kappler, J.W., Marrack, P., and Kedl, R.M. (2001). Observation of antigen-dependent CD8+ T-cell/dendritic cell interactions in vivo. Cell Immunol. *214*, 110–122.

Srinivas, S., Watanabe, T., Lin, C.-S., William, C.M., Tanabe, Y., Jessell, T.M., and Costantini, F. (2001). Cre reporter strains produced by targeted insertion of EYFP and ECFP into the ROSA26 locus. BMC Dev. Biol. *1*, 4.

Sun, D., Luo, M., Jeong, M., Rodriguez, B., Xia, Z., Hannah, R., Wang, H., Le, T., Faull, K.F., Chen, R., et al. (2014). Epigenomic profiling of young and aged HSCs reveals concerted changes during aging that reinforce self-renewal. Cell Stem Cell *14*, 673–688.

Viny, A.D., Ott, C.J., Spitzer, B., Rivas, M., Meydan, C., Papalexi, E., Yelin, D., Shank, K., Reyes, J., Chiu, A., et al. (2015). Dose-dependent role of the cohesin complex in normal and malignant hematopoiesis. J. Exp. Med. *212*, 1819–1832.

Wilson, A., Laurenti, E., Oser, G., van der Wath, R.C., Blanco-Bose, W., Jaworski, M., Offner, S., Dunant, C.F., Eshkind, L., Bockamp, E., et al. (2008). Hematopoietic stem cells reversibly switch from dormancy to self-renewal during homeostasis and repair. Cell *135*, 1118–1129.

Xie, H., Xu, J., Hsu, J.H., Nguyen, M., Fujiwara, Y., Peng, C., and Orkin, S.H. (2014). Polycomb repressive complex 2 regulates normal hematopoietic stem cell function in a developmental-stage-specific manner. Cell Stem Cell *14*, 68–80.